CHALMERS
UNIVERSITY OF TECHNOLOGY

Transmission Line Protection Using Dynamic State Estimation and Advanced Sensors: Experimental Validation

Citation for the original published paper (version of record):
Srivastava, A., Le, A., Steen, D. et al (2023). Transmission Line Protection Using Dynamic State Estimation and Advanced Sensors: Experimental
Validation. IEEE Transactions on Power Delivery, 38(1): 162-176.
http://dx.doi.org/10.1109/TPWRD.2022.3184479

(article starts on next page)

Transmission Line Protection Using Dynamic State Estimation and Advanced Sensors: Experimental Validation

Ankur Srivastava, *Student Member, IEEE,* Le Anh Tuan, *Member, IEEE,* David Steen, Ola Carlson, Omar Mansour, and Dennis Bijwaard

***Abstract*—This paper presents the experimental validation of a protection scheme for a transmission line based on dynamic state estimation along with the practical application of advanced sensors in this protection scheme. The scheme performs dynamic state estimation with high-frequency measurements provided by the sensors, assesses the operating condition (i.e., health) of the transmission line in real-time, and thereby determines the tripping signal whenever a fault is detected. The validation was carried out in two steps, first with simulation studies for a three-phase fault and then with the experimental implementation using a physical scaled-down model of a power system consisting of transmission lines, transformers, and loads. The simulation and validation results have shown that the scheme performs adequately in both normal and fault conditions. In the fault case with the experimental setup, the scheme could correctly detect the fault and send the trip signal to the line's circuit breakers with a total fault clearing time of approximately 65 milliseconds which is comparable to conventional protection methods. The average processing time for a measurement sample block is 12.5 milliseconds. The results demonstrate that this scheme and the sensors would work for transmission line protection which can avoid relay coordination and settings issues.**

***Index Terms*—Dynamic state estimation, experimental validation, phasor measurement unit, power system protection.**

I. Introduction

A. Motivation

PROTECTION against undesirable events is one of the important functions in power system operation. It is also important from the perspective of system reliability, continuity of power supply, and personnel safety. North American Electric Reliability Corporation (NERC) has reported that approximately 10% of protection operations are misoperations that lead to interruptions [1]. Across NERC from 2012 to 2014, 31% of misoperations occurred due to incorrect settings, 19% due to relay failures, and 13% due to communication failures which in total accounts for 63% of the total misoperations [1].

The conventional schemes employed for the protection of transmission systems include e.g., distance, pilot relaying, directional overcurrent, line differential, etc. There are some limitations associated with these protection schemes which might lead to misoperation. The work presented in [2] has identified the limitations of these protection schemes and also the protection gaps which exist in transmission systems. A few highlights related to the limitations of the conventional protection schemes are, i) Distance and directional overcurrent schemes require complex coordination and the simultaneous tripping of both ends is not possible, ii) Both pilot relaying and line differential schemes require communication infrastructure and its failure could lead to misoperation [2]. Although differential protection is successfully implemented and working in transmission systems, there still exist protection gaps such as relay desensitization due to capacitive currents in long transmission lines [3], detection of high impedance faults (especially in long transmission lines), and failure in case of communication loss.

Dynamic state estimation (DSE) based protection is one of the possible solutions to these challenges as it adapts to the operating conditions of the system in real-time and provides better visibility of the system status [4]. A feasibility study for such a protection scheme is presented in [5]. The study is further supported by its application for fault detection in a transmission line and capacitor bank. The detailed concept of this scheme along with its capabilities to improve zone protection, detection, and self-healing against hidden failures are discussed in [2]. The DSE-based protection is based on a generalized concept and has been applied to the protection of series compensated transmission line [6], transmission line fault classification [7], and several other components.

The more recent application of the DSE-based protection scheme includes the development of centralized substation protection in [8]. A microgrid protection scheme is developed using synchrophasor-based state estimation (SE) in [9]. A DSE-enabled protection scheme is proposed in [10] for large synchronous generators during out-of-step conditions. A novel fault location method utilizing DSE and gradient descent is proposed in [11] for transmission lines in modular multilevel converter-HVDC grids. A wide-area backup protection scheme is proposed in [12] which employs cubature Kalman filter-based DSE along with a few phasor measurement unit (PMU) measurements for acquiring full network observability. Despite the application of the different DSE versions in designing the protection scheme for power systems and their components, most of the research works have presented the simulation results and validation with the hardware-in-the-loop test. Therefore, validation of this scheme in a real environment is needed for technology advancement before it can actually be employed in power systems. The task force paper on DSE-based protection also identifies the practical implementation as a key research area in the future [13].

The work presented in this paper is financially supported by the following projects: i) UNITED-GRID - received funding from the European Community's Horizon 2020 Framework Programme under grant agreement no. 773717; ii) FLEXI-GRID - received funding from the European Community's Horizon 2020 Framework Programme under grant agreement no. 864048.

A. Srivastava, L. A. Tuan, D. Steen, and O. Carlson are with the Division of Electric Power Engineering, Department of Electrical Engineering, Chalmers University of Technology, Gothenburg, 412 96, Sweden (e-mail: ankur.srivastava@chalmers.se.)

O. Mansour and D. Bijwaard are with Smart State Technology BV, Hengelo, The Netherlands.

DSE-based protection requires real-time measurements as the input. With the advent of PMU technology in the 1980s and development thereafter, it has evolved as one of the reliable solutions for real-time measurements. PMU finds huge application in the monitoring, operation, and protection of power systems. However, most commercial PMUs have little scope for third-party users to modify and develop their control algorithms. In this context, this paper proposes an affordable measurement solution (advanced sensors) with a scalable and modular design, web interface feature, secure edge computing, and development in an open platform that could be deployed at all voltage levels for further enhancement of the grid's monitoring, operation, and protection.

B. Contributions

This paper aims to perform an experimental validation of a dynamic state estimation-based protection scheme (DSEBPS) developed in [2] for a transmission line using affordable advanced sensors. The work presented in the paper involves implementation and execution of the existing method, performing additional simulation case studies thereafter and setting up the experimental setup followed by the validation of the method. The validation is performed using an open platform approach which provides enough space for the researchers to modify or add new features in the future. The experimental setup used for validation utilizes the real-time measurements provided by advanced sensors, which are one of the essential inputs for the validation of the scheme.

The main contributions of the paper which is carried out within the scope of the UNITED-GRID project [14], can be summarized as follows:

- Development of an affordable and reliable real-time measurement solution i.e., advanced sensors and associated control platform, for the enhancement of the grid monitoring capability with a dedicated commercial roll-out strategy.
- Preparation of the experimental setup to validate DSEBPS for a transmission line including the setup and proper interface of circuit breakers, communication requirements, and advanced sensors.
- Implementation of DSE algorithm in Python and integration with the measurements' system provided by advanced sensors to create an open platform for testing in Python.
- Finally, carrying out the test and evaluating the results to validate the practical feasibility of DSEBPS scheme for a transmission line and to advance the maturity of the sensor technology.

II. Transmission Line Protection Based on Dynamic State Estimation

A. Brief Introduction

DSEBPS can be regarded as the generalization of differential protection. The basic concept used in this scheme is the obeying of all physical laws including Kirchhoff's voltage and current laws, by the transmission line. If any of these laws are violated by the transmission line, then it confirms the faulty condition. The biggest advantage associated with this scheme is the simplification of the protection settings and elimination of the coordination with other components [5].

DSEBPS uses DSE which performs the dynamic modelling of all physical laws that the transmission line should satisfy. The dynamic model is constantly observed by DSE and any violations of laws (abnormality) are apprehended. The analog signals such as voltage, current, etc., and digital signals such as circuit breakers, etc., are measured from the transmission line. DSE utilizes these measurements along with the dynamic model and estimates the operating states of the transmission line. After estimating the states, the Chi-square test is performed to examine the consistency of the estimates with the measurements or goodness of fit between the dynamic model and measurements. The goodness of fit can be interpreted to determine the transmission line health and obtain the confidence level. The high confidence level indicates normal operation, while a low level indicates abnormal operation [2].

B. Problem Formulation

A generic π-model for a transmission line has been adapted from the model of distribution line which is developed in [15] by using the transmission line parameters. The mathematical problem formulation is divided into the following sub-sections:

1) Dynamic Model: The transmission line dynamic model is obtained through the algebraic quadratic companion form and quadratic integration (QI) method. The schematic of a three-phase transmission line is presented in Fig. 1. The resistances and reactances of each phases are represented as (R_A, R_B, R_C) and (L_A, L_B, L_C), respectively. The shunt capacitances for each phases are represented as (C_A, C_B, C_C). The sending end currents represented as (i_A, i_B, i_C), receiving end currents as (i_a, i_b, i_c), and receiving end voltages as (v_a, v_b, v_c), are considered as the measurements, while the sending end voltages (v_A, v_B, v_C) and series branch currents (i_{dA}, i_{dB}, i_{dC}) are considered as the estimated variables. (G_A, G_B, G_C) are used for stability purpose in the numerical integration and are not a part of the physical line model. They help in avoiding the expansion of round-off errors or fluctuations in input data which could lead to substantial deviation of the final answer when numerical integration is applied in differential equations [16]. The model equations for the A-phase can be written as [17]:

$$v_a = v_A - R_A i_{dA} - L_A \frac{di_{dA}}{dt} \tag{1}$$

$$i_A + G_A v_a = i_{dA} + G_A v_A + C_A \frac{dv_A}{dt} \tag{2}$$

$$i_a - G_A v_a - C_A \frac{dv_a}{dt} = -i_{dA} - G_A v_A \tag{3}$$

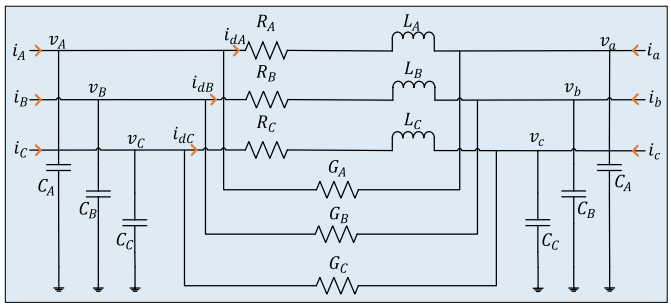

Fig. 1. Schematic of a three-phase transmission line.

Equations (1)−(3) along with B and C phase equations can be condensed into the following form:

$$R_1 z + R_2 \frac{dz}{dt} = S_1 x + S_2 \frac{dx}{dt} \tag{4}$$

where z is the measurement vector and given as $[i_A\ i_B\ i_C\ i_a\ i_b\ i_c\ v_a\ v_b\ v_c]$, x is the state vector and given as $[v_A\ v_B\ v_C\ i_{dA}\ i_{dB}\ i_{dC}]$, and R_1, R_2, S_1, and S_2 are constant matrices made up of line parameters value. If mutual coupling between the different phases is considered, then equations (1)−(3) and subsequently R_1, R_2, S_1, and S_2 matrices should be updated accordingly. It should be noted that the ground path is not incorporated in the transmission line model as the type of grounding and its configuration is outside the protection zone of a transmission line and thus it shall not have an impact on DSEBPS.

QI method is used to simplify the differential equations which are involved in the formulation. In QI method, for one integration interval, the function varies quadratically and this leads to higher accuracy as compared to other methods. The application of QI method in (4) over the time intervals $[t-k, t-k/2]$ and $[t-k, t]$, leads to the following equation:

$$H_1 \begin{bmatrix} z(t) \\ z\left(t-\frac{k}{2}\right) \end{bmatrix} = H_2 \begin{bmatrix} x(t) \\ x\left(t-\frac{k}{2}\right) \end{bmatrix} - H_3 \left[z(t-k)\right] - H_4 \left[x(t-k)\right] \tag{5}$$

where k is one-time step of QI method, and H_1, H_2, H_3, and H_4 are the coefficient matrices defined as follows.

$$H_1 = \begin{bmatrix} \frac{k}{6}R_1 + R_2 & \frac{2k}{3}R_1 \\ -\frac{k}{24}R_1 & \frac{k}{3}R_1 + R_2 \end{bmatrix}, H_2 = \begin{bmatrix} \frac{k}{6}S_1 + S_2 & \frac{2k}{3}S_1 \\ -\frac{k}{24}S_1 & \frac{k}{3}S_1 + S_2 \end{bmatrix}$$

$$H_3 = \begin{bmatrix} \frac{k}{6}R_1 - R_2 \\ \frac{5k}{24}R_1 - R_2 \end{bmatrix}, H_4 = \begin{bmatrix} -\frac{k}{6}S_1 + S_2 \\ -\frac{5k}{24}S_1 + S_2 \end{bmatrix}$$

Restructuring (5), leads to the standard form of the state estimator and can be given as:

$$\begin{bmatrix} z(t) \\ z\left(t-\frac{k}{2}\right) \end{bmatrix} = H \begin{bmatrix} x(t) \\ x\left(t-\frac{k}{2}\right) \end{bmatrix} + C \tag{6}$$

where $H = H_1^{-1}H_2$, $C = -C_1\left[z(t-k)\right] - C_2\left[x(t-k)\right]$, $C_1 = H_1^{-1}H_3$, $C_2 = H_1^{-1}H_4$.

2) State Estimation Algorithm: The most common approach for the solution of SE i.e., the weighted least square (WLS) algorithm is used to solve SE problem. The linear version of the WLS algorithm can be stated as:

$$z = Hx + \eta \tag{7}$$

where z represents the measurement vector consisting of voltages and currents, H represents the Jacobian matrix, x represents the state vector and η represents the measurement error vector.

The objective function of SE can be defined as the minimization of the following function:

$$J = (z - H\hat{x})^T R^{-1} (z - H\hat{x})$$
$$J = \eta^T R^{-1} \eta \tag{8}$$

where $\hat{x}$ is the WLS estimate and R^{-1} is the diagonal weight matrix and defined as $diag\left(\sigma_1^2, \sigma_2^2, \sigma_3^2, \ldots.., \sigma_m^2\right)$.

The expression for the WLS estimate comes out as:

$$\hat{x} = \left(H^T R^{-1} H\right)^{-1} \left(H^T R^{-1} z\right) \tag{9}$$

3) Chi-square Test: The following steps are performed for the Chi-square test using the WLS SE algorithm:

- Calculate the SE objective function J using (8).
- Checkup with the Chi-square distribution table to quantify the confidence level which requires the degree of freedom (d) and SE objective function J, as inputs. The degree of freedom is calculated as $d = m - n$, where m is the number of measurements and n is the number of state variables.

4) Confidence Level: The confidence level (h) in the transmission line health is evaluated based on the goodness of fit between the dynamic model and measurements obtained from the Chi-square test as below:

$$h = 1 - p_{[\chi^2 \leqslant J]} \tag{10}$$

5) Threshold Value and Low Pass Filter: A threshold value is selected for the objective function such that the confidence level remains high during the normal operating conditions. It is required as there exists a slight mismatch between the measurements and their estimated values during the normal operating conditions and thus the objective function is evaluated as non-zero finite values. The threshold for the objective function is selected based on the range of objective function obtained during steady-state conditions with due consideration of measurement uncertainties as well as possible variation in system configurations. In addition to the threshold value, a low pass filter as presented in (11) is employed for smoothing the objective function curve.

$$J^f_{new} = (\alpha \times J) + [(1-\alpha) \times J^f_{previous}] \tag{11}$$

where, J and J^f are original and new objective functions, respectively, and α is the smoothing factor ranging between 0 and 1. Based on the experience from case studies with different values of α, it is taken as 0.001 in this work. The objective function presented in all the following case studies in the paper includes the threshold value and application of a low pass filter. In general, the threshold value that could work for most of the cases could be achieved by simulating the most credible fault cases e.g., maximum fault current, and then verifying that it should work with other cases e.g., minimum fault current considering the weakest source and highest fault impedance and also external faults. It should also be verified that the threshold level should not trigger the trip signal in high load conditions, as well as for external faults, current transformers (CTs) and voltage transformers (VTs)/coupling capacitor voltage transformers (CCVTs) errors, and/or saturation. From the experience of simulations with different faults studied in this paper for a 150-km long transmission line with an operating

voltage of 400 kV (scaled down model) and maximum measurement uncertainties in the range between 0.02% and 0.03%, the threshold value shall range between 2.0E6 and 2.5E6.

III. Advanced Sensors Description

Advanced sensors (AdvSens) have been continuously developed by Smart State Technology [18].

A. Features

AdvSens provide high-quality (both synchrophasor and sampled) measurements of the grid. They are capable of providing high-speed sampling with a low signal-to-noise ratio. The analog to digital converters (ADC) sampling system, which is locked to global positioning system (GPS) time, generates both phase and magnitude information.

B. System Architecture

The system architecture of AdvSens consists of a time beacon transmitter, voltage and current sensors, embedded computer, and data aggregation units (referred to as smart nodes).

1) Time Beacon Transmitter: Its function is to broadcast wired or wireless-time information, based on the GPS received pulse per second (PPS) signal and time of day NMEA messages, to a cluster of AdvSens. AdvSens use this time information to synchronize their sampling system and obtain synchronized measurements of voltage and current signals which are then digitized, processed, and transmitted to smart nodes. It allows a cluster of AdvSens to discipline their ADC with the received 1 second PPS signal and synchronize their measurements. Thus, it acts as a grandmaster clock for the cluster of AdvSens to have global synchronized measurements.

2) Voltage and Current Sensors: There are two types of AdvSens i.e., voltage and current sensors. The voltage sensors can have a measurement range up to 800 V (230 V nominal) and make use of signal transformers, while the current sensors make use of split-core CTs and have a measurement range up to 400 A.

3) Embedded Computer: The embedded single-board computer (SBC) in AdvSens is an ARM-based low power and low-cost processing platform. The SBC runs Linux as an operating system and contains drivers for receiving the synchronized ADC samples and hosts the open platform software architecture for the creation and processing of measurements.

4) Smart Nodes: Smart nodes are the data aggregators of the system, which hosts the transmission line dynamic model. They collect the measurement data from AdvSens and can perform calculations.

C. Calibration and Accuracy

The raw ADC samples may suffer from inaccuracies due to component tolerances and the non-linearity of the signal transducers. Also, the measured ADC counts are required to be converted to signal values. The sensor calibration DSP converts the ADC counts to accurate signal values. For accurate conversion, the calibration DSP uses a table that maps measurement ADC counts to actual signal values. The table stores various calibration points to cover the full measurement range of AdvSens including the measurement regions where AdvSens may exhibit non-linearity (typically in the initial low measurement region and in the saturation region of the transducer CTs).

IV. Case Study

A. Description

The case study considered for the simulation of DSEBPS consists of a transformer, six π-sections of a transmission line (each π-section corresponds to 150-km of a 400 kV line), and a resistive load which is a physical setup available at Chalmers power system laboratory. The motivation to choose this test system is the representation of a multi-section line (similar to a radial distribution system) which will have multiple relays that needs to be coordinated. Additionally, more π-sections will increase the length of the transmission line which help to reduce the fault current. The parameters and the values of the components which are considered in the simulation are presented in Table I.

TABLE I
Parameters and the Values of the Simulation Components

Parameter		Value
Nominal grid voltage		400 V
Nominal grid frequency		50 Hz
Each π-section	Series resistance	0.052 Ω
	Series inductance	3.033 mH
	Shunt capacitance	46 μF
Resistive load		9 kW

B. Simulation Setup

The simulation for the case study is performed in MATLAB Simulink (R2020b version). The single-line diagram of the network is presented in Fig. 2. As shown in Fig. 2, the simulation network consists of six π-sections which are connected to the main grid at one end and 9 kW resistive load on the other end.

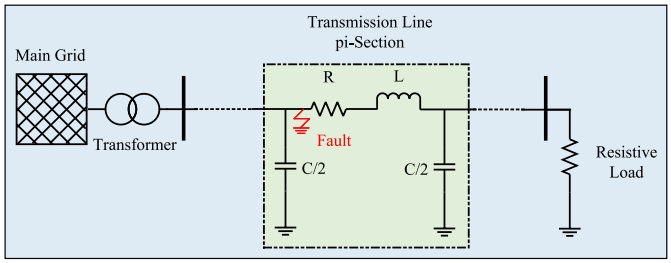

Fig. 2. Single-line diagram of the simulation setup for a fault.

For DSEBPS, the sending end currents (i_A, i_B, i_C), receiving end currents (i_a, i_b, i_c), and receiving end voltages (v_a, v_b, v_c) are taken as the measurements, while the sending end voltages (v_A, v_B, v_C) and series branch currents (i_{dA}, i_{dB}, i_{dC}) are taken as the estimated variables, as shown in Fig. 1. This selection is done on an arbitrarily basis except for the series branch currents (i_{dA}, i_{dB}, i_{dC}) due to their physical unavailability in the laboratory setup. In the case of a meshed network, the selection should be made such that SE remains an over-determined problem. The estimated values of the measurements are calculated back through the estimated

variables so that a comparison could be made between the measurements and their estimated values. The comparison between the measurements and their estimated values is used for the calculation of the SE objective function. Additionally, as the measured values of the estimated variables are not available, they cannot be compared and hence not presented in the plots.

The transmission line is modelled using the lumped model instead of the distributed model. The corrections due to distributed model are more significant with the increased line length (more than 200 km). The lumped model is preferred in this work as the series branch currents (i_{dA}, i_{dB}, i_{dC}) could not be calculated in a distributed model. However, the impact of distributed parameters on DSEBPS will be very limited in the present case study due to short line length.

V. Simulation Results

A. Three-phase Fault with Resistive Load

The simulation is run for 0.15 seconds and the measurement sampling rate is taken as 1E-6. The sampling rate corresponds to the rate at which a continuous signal is discretized to generate sampled values. The sampling rate of 1E-6 translates to a sampling frequency of 1000 kHz or 1 MHz. A three-phase fault is created for 40 milliseconds initiated at 0.04 seconds and cleared at 0.08 seconds. The simulated measurements from Simulink are saved into the workspace and are provided as inputs to the script of the DSE-based protection scheme executed in MATLAB. The simulated measurements are compared with their estimated values calculated using the estimated variables. The three-phase simulated measurements along with their estimated values are presented in Fig. 3. Only the case for a three-phase fault is presented here, the method works with all other types of faults, due to the fact that estimates do not depend on the fault type, and thus the algorithm will work as intended.

It can be seen from Fig. 3 that during the normal operating conditions from 0 to 0.04 seconds the simulated measurements and their estimated values are in concurrence, while when the fault occurs (between 0.04 and 0.08 seconds), the simulated measurements and their estimated values have substantial differences. The reason behind the inconsistency is due to the consideration of steady values of system parameters (e.g. constant frequency as 50 Hz) during the fault conditions. The system returns to normal conditions soon after the fault is cleared. The original objective function, filtered objective function, and confidence level are presented in Fig. 4. A threshold value of 2.22E6 is used to set the objective function to zero during normal conditions based on the explanation provided in Section II-B. Fig. 4 shows that values of the filtered objective function are low during the normal conditions (0 to 0.04 seconds), while they rise substantially high during the fault condition (0.04 to 0.08 seconds). Based on the objective function, the Chi-square test is performed which gives a high confidence level (indicating goodness of fit between the dynamic model and measurements) during the normal condition. During the fault conditions, the high values of objective function lead to a low confidence level. Based on the low confidence level a trip signal is generated and sent to the circuit breakers. Additionally, a separate case study with the inclusion of CTs and CCVTs was performed which showed that their transient response does not have an impact on the DSEBPS performance. In this case study the fault was created very close to the CCVTs location leading to transients. DSEBPS performed as intended under this condition as well and the trip signal was generated successfully.

An additional case study was performed with an inductive

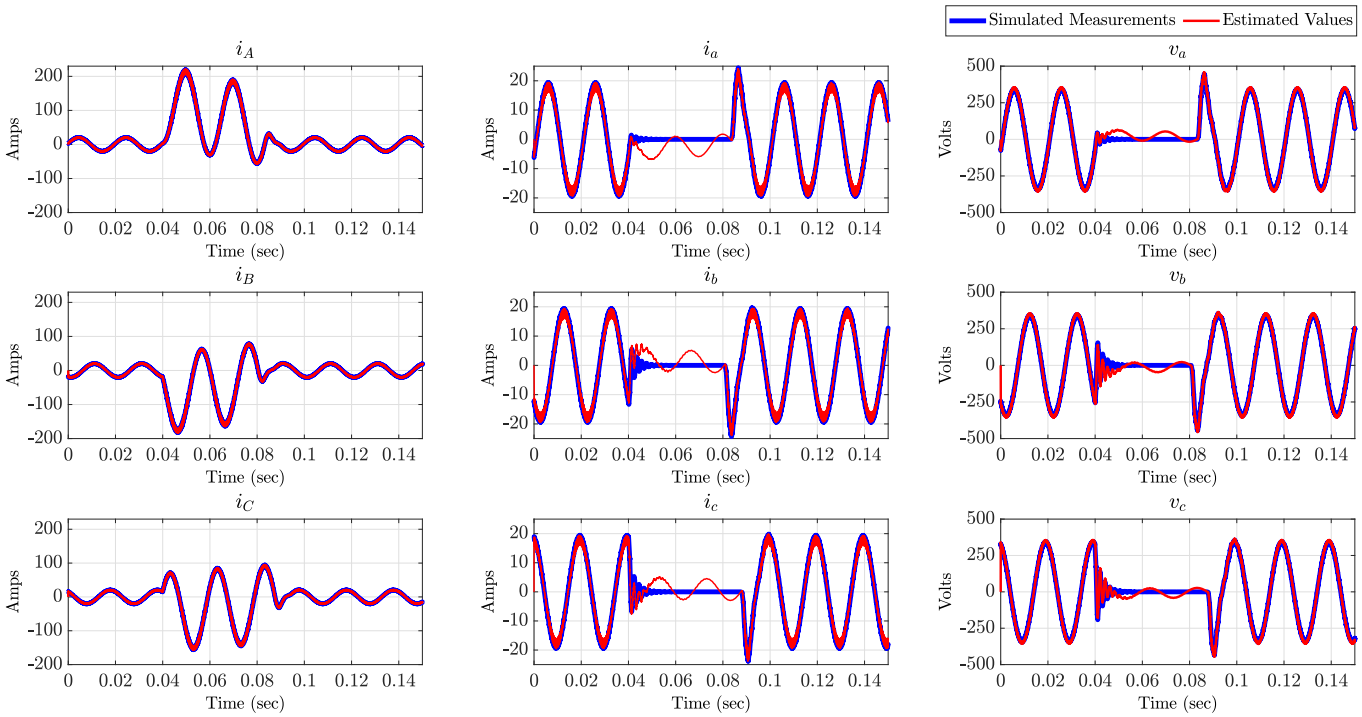

Fig. 3. MATLAB Simulink results in terms of simulated measurements and their estimated values of the sending end currents (i_A, i_B, i_C), receiving end currents (i_a, i_b, i_c), and receiving end voltages (v_a, v_b, v_c) for a three-phase fault.

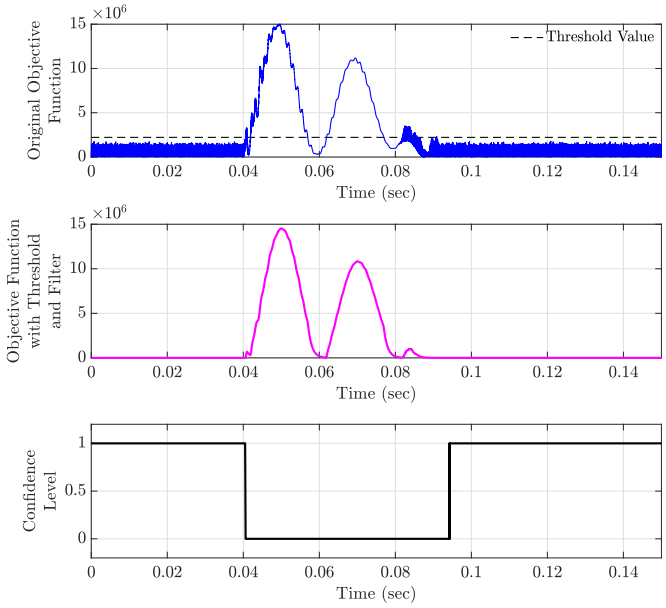

Fig. 4. MATLAB Simulink results in terms of original objective function, filtered objective function, and confidence level for a three-phase fault.

load of 0.8 lagging power factor to analyze the impact of different load conditions on DSEBPS using the same test setup. The simulation results showed that the method performed satisfactorily and successfully issued a trip signal in response to the fault. The main changes were observed in the current and voltages signals which showed sluggish response as compared with the resistive load but it did not have an impact on the confidence level and trip signal generation.

B. High Impedance Fault

A high impedance fault could be described as the one where the fault impedance is high and that leads to reduced fault current, sometimes close to or less than normal loading current. DSEBPS is examined with the same test setup as explained in Section IV using the MATLAB software by creating a three-phase fault with equivalent fault impedance of 25 Ω for 40 milliseconds initiated at 0.04 seconds and cleared at 0.08 seconds. Due to space limitations, only the simulation results with equivalent fault impedance of 25 Ω are presented here. However, the simulations were carried out with different values of equivalent fault impedances such as 15 Ω, 5 Ω, 1 Ω, and 0.1 Ω. These case studies showed that during the fault conditions the sending end currents reach a higher peak, while the receiving end currents and receiving end voltages increases with the increase in equivalent fault impedance.

The sending end current, receiving end current, and receiving end voltage for phase A with 25 Ω fault impedance are presented in Fig. 5. The voltages and currents for phases B and C were similar to phase A. It can be seen from Fig. 5 that the receiving end voltage and receiving end current during fault conditions are in the same range as normal operating conditions. In the case of sending end current, a small transient (peak value of around 30 Amperes) could be seen due to the addition of a small fault current component along with load current. Despite the absence of a large fault current (due to high fault impedance) and transients, a non-

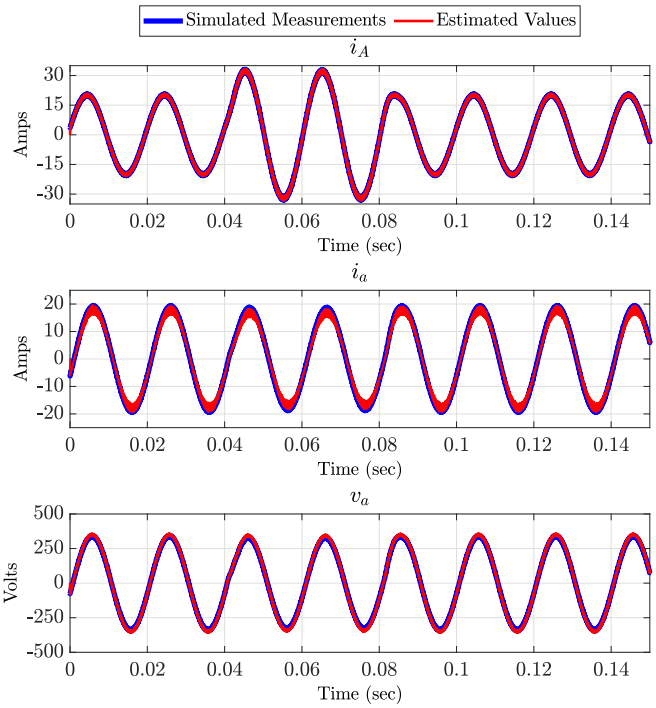

Fig. 5. MATLAB Simulink results in terms of simulated measurements and their estimated values of the sending end current (i_A), receiving end current (i_a), and receiving end voltages (v_a) for a high impedance fault.

conformity exists between the simulated measurements and their estimated values. Due to this non-conformity between the simulated measurements and their estimated values, the objective function sees a spike (smaller as compared to a zero impedance fault), while keeping the same threshold value (i.e., 2.22E6). As the objective function goes high, correspondingly the confidence level goes low (i.e., 0), as can be observed in Fig. 6. Thus, a trip signal is generated during fault and sent to the breakers.

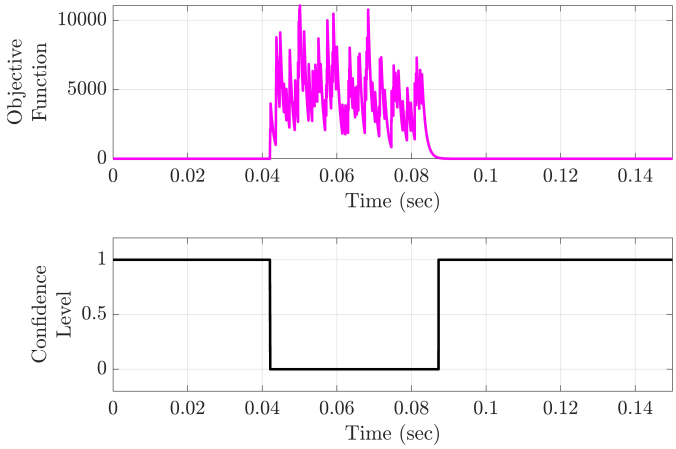

Fig. 6. MATLAB Simulink results in terms of objective function and confidence level for a high impedance fault.

C. External Fault

An external fault is the one that occurs outside the protection zone and the protection scheme should identify it as an external fault such that a trip signal should not be issued. DSEBPS is examined with the same test setup as explained in Section IV by creating an external fault (just outside the

protected transmission line) for 40 milliseconds initiated at 0.04 seconds and cleared at 0.08 seconds.

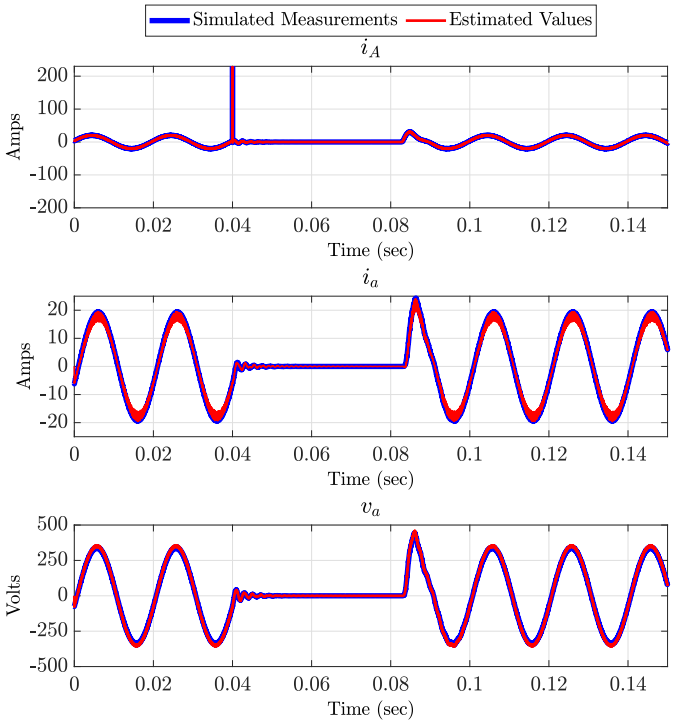

Fig. 7. MATLAB Simulink results in terms of simulated measurements and their estimated values of the sending end current (i_A), receiving end current (i_a), and receiving end voltage (v_a) for an external fault.

Fig. 7 shows that the transients occur in the simulated measurements of sending end currents, receiving end voltages, and receiving end currents due to an external fault. Despite the transients in the simulated measurements, the estimated values are in concurrence with the measurements. Due to this concurrency between the simulated measurements and their estimated values, the objective function remains below the set threshold value and hence the confidence level remains high (i.e., 1) as can be observed in Fig. 8, and hence a trip signal is not generated in case of an external fault (which is intended). Thus, DSEBPS discriminates against the external fault and does not issue a trip signal.

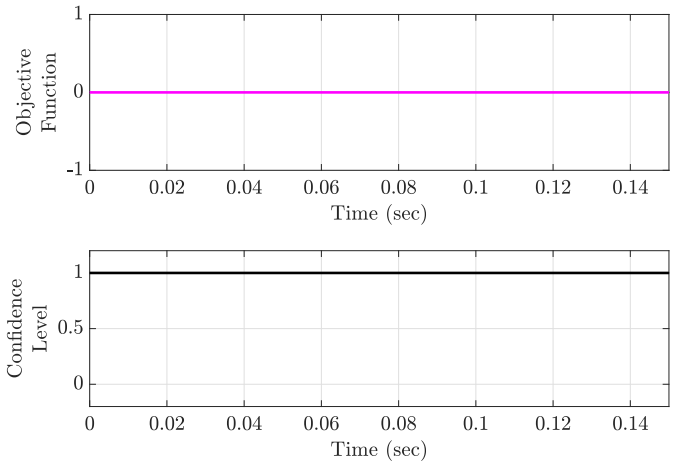

Fig. 8. MATLAB Simulink results in terms of objective function and confidence level for an external fault.

D. Fault Current Fed from Both Ends

In case of meshed network, fault current is fed from both ends of the transmission line. DSEBPS is examined with the same test setup as explained in Section IV by adding a generator on the receiving end. A three-phase fault is created for 40 milliseconds initiated at 0.04 seconds and cleared at 0.08 seconds.

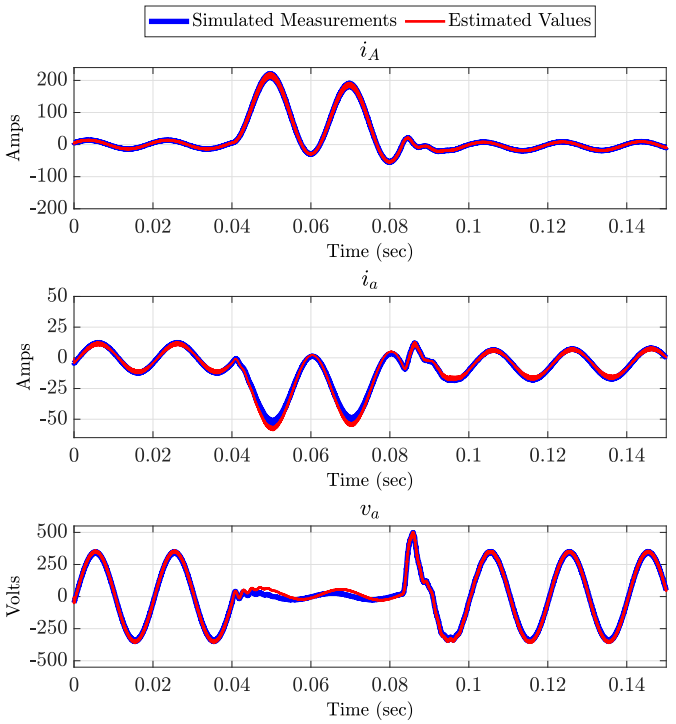

Fig. 9. MATLAB Simulink results in terms of simulated measurements and their estimated values of the sending end current (i_A), receiving end current (i_a), and receiving end voltage (v_a) for a fault current fed from both ends.

Fig. 9 shows that the measurements and the estimated values of receiving end current for phase A (i_a) goes high during the fault conditions unlike the previous fault due to consideration of a fault current fed from both ends. The contribution of the receiving end generator depends on the rating of the generator. In case of the receiving end voltage for phase A (v_a), it

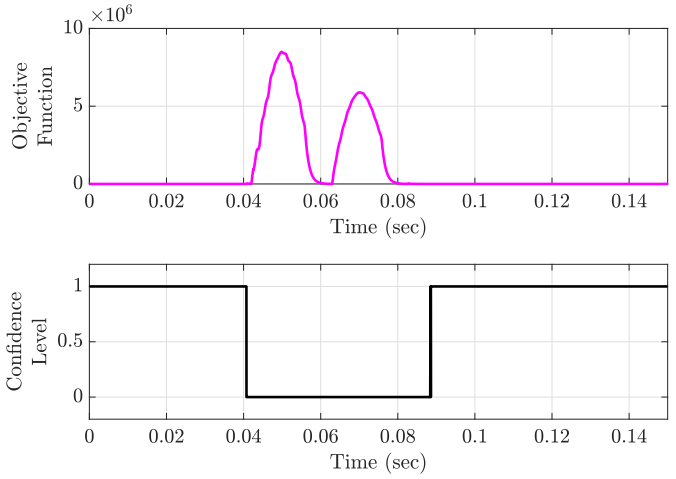

Fig. 10. MATLAB Simulink results in terms of objective function and confidence level for a fault current fed from both ends.

reduces during the fault but not until zero unlike the fault current fed from one end. Further, it can be seen from Fig. 10 that as soon as the three-phase fault occurs at 0.04 seconds, the objective function goes high and subsequently the confidence level goes low (i.e., 0). Thus, a fault in the meshed network is successfully detected by DSEBPS.

E. Transmission Line Parameter's Uncertainty

There is uncertainty associated with transmission line parameters which could have an impact on DSE accuracy or any other type of SE, which uses line parameters as inputs. The line parameters could vary ranging between 1% and 20% [19]. Based on this range, a case study is performed where all line parameters (resistances, inductances, and capacitances) are varied $\pm 10\%$. The same test setup as explained in Section IV is employed by creating a three-phase fault for 40 milliseconds initiated at 0.04 seconds and cleared at 0.08 seconds. To compare the results, the newly obtained objective function is plotted with the objective function obtained with original line parameters, as shown in Fig. 11.

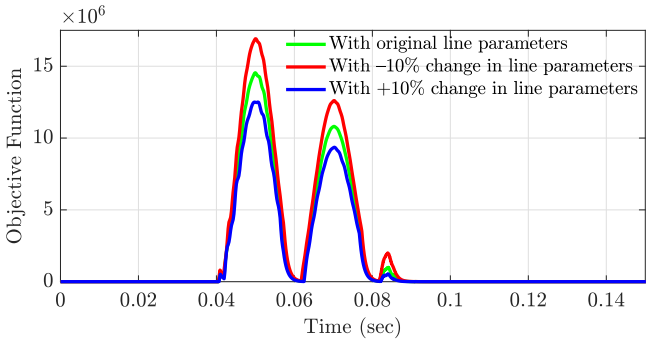

Fig. 11. A plot of the objective function with different values of transmission line parameters accuracy.

It can be seen from Fig. 11 that due to uncertainties the main change is visible in the peaks of the objective function. The difference in peaks shows a higher mismatch between the measurements and their estimated values due to uncertainties introduced in the transmission line parameters. However, it does not impact the results of DSEBPS as minimal changes are observed in objective function immediately after the fault initiation (around 0.04 seconds).

Thus, it can generally be concluded based on the simulation studies that DSEBPS has robust performance and works satisfactorily under different load conditions, high impedance fault, and external fault. Further, DSEBPS works also with limited uncertainty in transmission line parameters.

VI. Validation Using Experimental Setup

This section explains the application of AdvSens, description of the laboratory, details of the experimental setup, implementation of the scheme, data flow process, obtained results and discussion, and comparison with the simulation results.

A. Application of AdvSens

AdvSens provides the real-time sampled measurements which serve as input to DSEBPS. The accuracy and sampling frequency of the measurements are important requirements for timely and accurate detection of the fault condition. The high-frequency sampled measurements are required to capture any dynamical change in the transmission line. The motivation to choose sampled measurements over phasors is that the phasors are updated at a lower frequency (usually around 50 to 100 frames per second for a 50 Hz system and 60 to 120 frames per second for a 60 Hz system) when compared to sampled measurements. With reduced updating time of phasors, the accuracy to capture any transient event reduces. The sampled measurements are provided at a sampling rate of 4 kHz. By evaluating case studies with different data acquisition rates, the rates ranging between 2 kHz to 5 kHz are found to be optimal. The acquisition rates less than 2 kHz could negatively impact the capturing of real-time picture of a transmission line due to low refresh rate, while the acquisition rates more than 5 kHz gets limited due to the increased need for computation. The measurement vector includes the voltages and currents from the terminals of the transmission line and is represented as z in (7).

B. Laboratory Description

The Chalmers power systems laboratory hosts an experimental setup of an accurate scaled-down model of a simple power system. It consists of a synchronous generator driven by a DC motor, two transformers, six π-sections of a transmission line, and loads. Each π-section in the setup corresponds to 150 km of a 400 kV line. The whole setup operates at a nominal voltage of 400 V with a nominal grid frequency of 50 Hz. The parameters of each π-section in the setup are presented in Table I.

C. Experimental Setup

The experimental setup used in the validation utilizes the six π-sections of a transmission line connected through the local three-phase 400 V Chalmers campus grid at one end and a 9 kW resistive load on the other end. The setup also includes three AdvSens which measure the sending end currents (i_A, i_B, i_C), receiving end currents (i_a, i_b, i_c), and receiving end voltages (v_a, v_b, v_c). The current measuring AdvSens uses split-core CTs which are part of the measurement class and are calibrated and tested for the required current range of the test setup. The current range covers both normal operating current and maximum fault current, while the voltage measuring AdvSens directly measures the voltages without using the VTs/CCVTs. The picture of the experimental setup used in this work is shown in Fig. 13.

D. Implementation

The implementation diagram of DSEBPS with the experimental setup is shown in Fig. 12. AdvSens are installed at the transmission line, which provides the GPS-synchronized real-time sampled measurements and received in a smart node. The smart node used in this setup is a laptop whose configuration is presented in Table II. The smart node processes the measurements along with the transmission line dynamic model to perform the DSE. The state estimates are obtained through DSE and then the Chi-square test is performed to obtain the goodness of fit between the dynamic model and measurements.

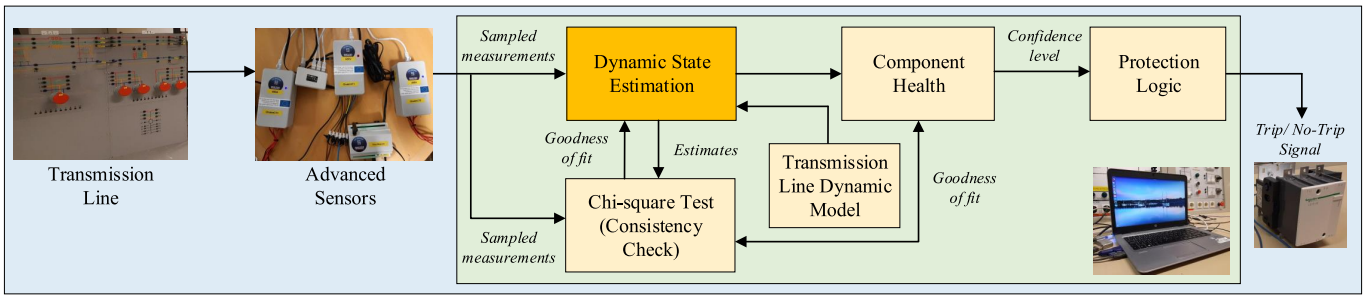

Fig. 12. Implementation diagram of DSEBPS with experimental setup at Chalmers power systems laboratory.

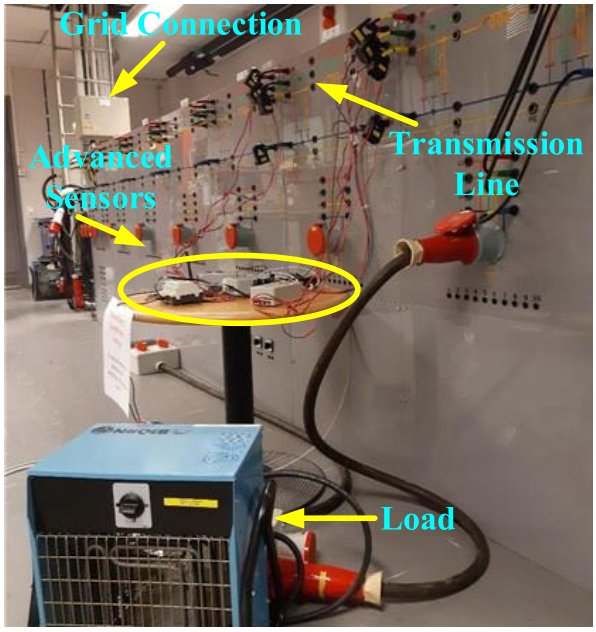

Fig. 13. Picture of the experimental setup at Chalmers power systems laboratory.

The health condition is then derived based on the results of the Chi-square test which provides the confidence level and helps in designing the protection logic whether to generate a trip signal or not.

TABLE II
CONFIGURATION DETAILS OF THE SMART NODE

Component	Configuration Details
Memory	15.5 GiB
Processor	IntelR CoreTM i7-6600U CPU @ 2.60 GHz × 4
Graphics	IntelR HD Graphics 520 (Skylake GT2)
Disk	503 GB
Ubuntu Version	Ubuntu 18.04.3 LTS
Python3 packages	Mainly NumPy (1.16.4) and SciPy (0.19.1)

E. Data Flow Process

The data flow process diagram for the experimental setup is presented in Fig. 14, which explains the process of data flow from the measurement point until the trip signal. The setup executes two different digital signal processes, the first performs DSE and Chi-square test (abbreviated as D_1) and the second performs the confidence level calculation (D_2). Also, three real-time data (rtd) plots are shown, the first plots the measurements and their estimated values (R_1), the second plots the objective function (R_2), and the third plots the confidence level (R_3).

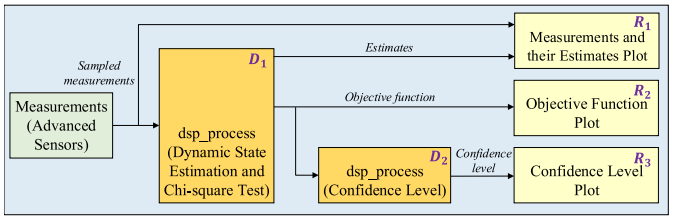

Fig. 14. Data flow process diagram for the experimental setup at Chalmers power systems laboratory.

F. Validation Results and Discussion

The single-line diagram of the experimental setup is presented in Fig. 15. The validation results using the setup in terms of measurements and their estimated values are presented in Fig. 16. The measurements, state estimates, objective function, and confidence level are continuously obtained and their values are updated and plotted in R_1, R_2, and R_3 plots, respectively.

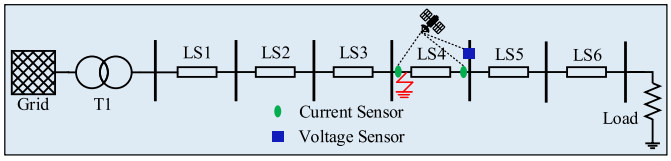

Fig. 15. Single-line diagram of the experimental setup with the location of AdvSens and fault.

It can be seen from Fig. 16, that during the normal operating conditions (until 2.795 seconds), the measurements and their estimated values (sending end currents (i_A, i_B, i_C), receiving end currents (i_a, i_b, i_c), and receiving end voltages (v_a, v_b, v_c)) conform with each other. Correspondingly, the objective function is low and the confidence level is high, as shown in Fig. 17. The obtained results confirm that measurements and estimated values should be in conformity during the healthy operation, thanks to the correct dynamic modelling of the transmission line.

Thereafter, a three-phase short-circuit fault is created for 40 milliseconds at the sending end of the fourth π-section, as shown in Fig. 15. The fault time settings could be set by using a timer and then a push button is pressed which creates the fault for a set time. This mechanism then auto clears the fault. The timer settings and the push button can be seen in

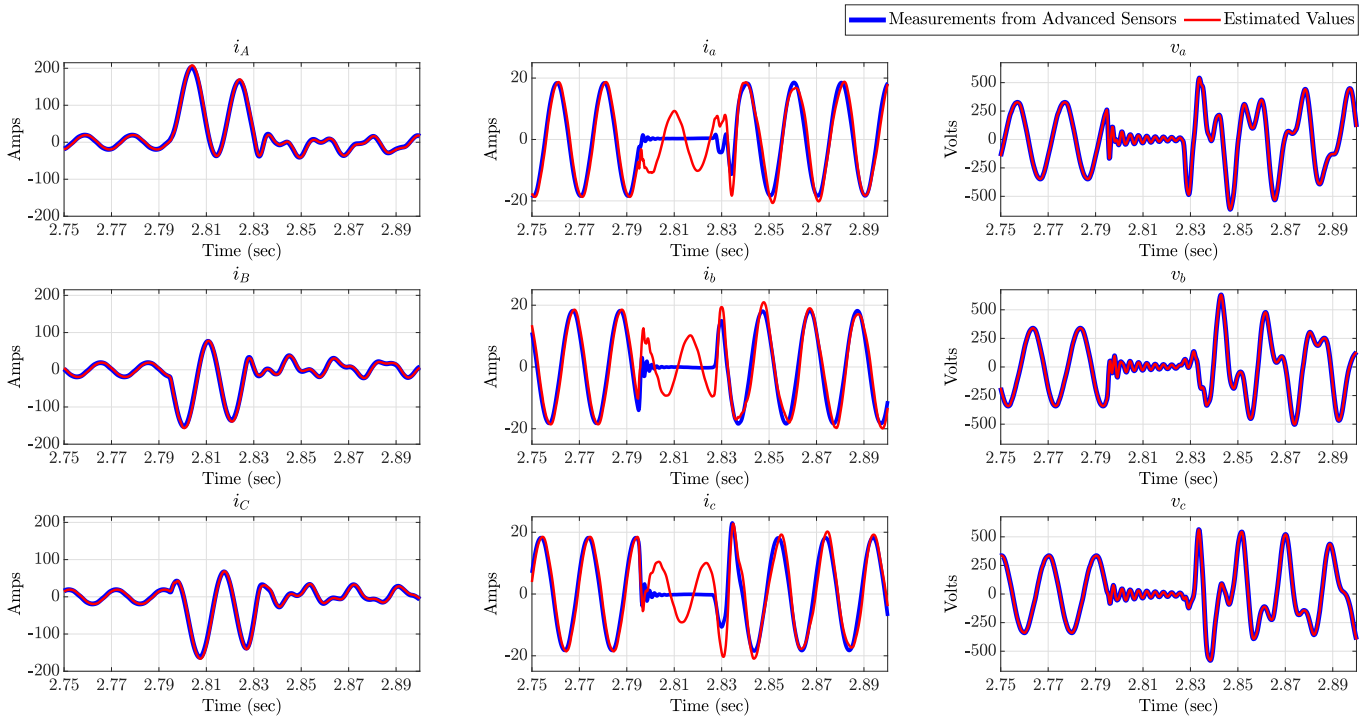

Fig. 16. Experimental validation results in terms of measured and estimated values of the sending end currents (i_A, i_B, i_C), receiving end currents (i_a, i_b, i_c), and receiving end voltages (v_a, v_b, v_c).

Fig. 18(a). As can be seen from Fig. 16, that during the fault condition (approximately between 2.795 and 2.835 seconds), the sending end currents (i_A, i_B, i_C) becomes high, while the receiving end currents (i_a, i_b, i_c) and receiving end voltages (v_a, v_b, v_c) tends towards zero due to the short-circuit fault. The objective function goes high and the confidence level goes low, during the fault condition (approximately between 2.795 and 2.835 seconds), as can be seen in Fig. 17. The non-conformity between the measurements and their estimated values leads to a high value of the objective function.

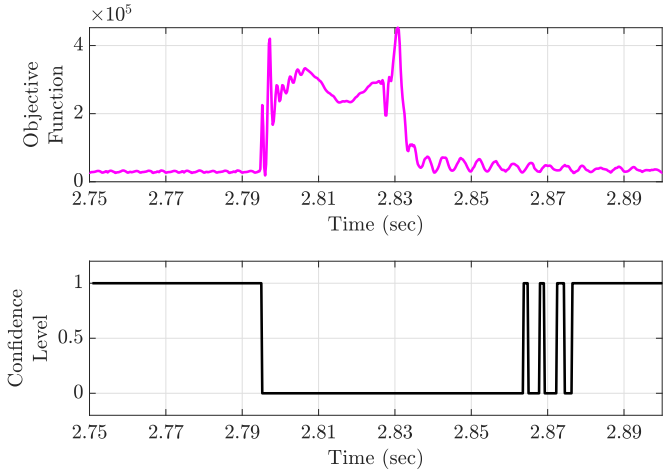

Fig. 17. Experimental validation results in terms of objective function and confidence level.

G. Trip Signal

The trip signal is generated based on the consistency of the objective function signal. The objective function signal is observed for three consecutive samples implying that if it remains above the threshold value for three consecutive samples, then confidence level goes down and a trip signal is given to the breaker for operation [20]. The motivation for observing the three consecutive values of the objective function signal is to obtain the trip decision with increased reliability. A USB latch device is used as an interface between the smart node and the circuit breaker. The trip signal setup is shown in Fig. 18(b).

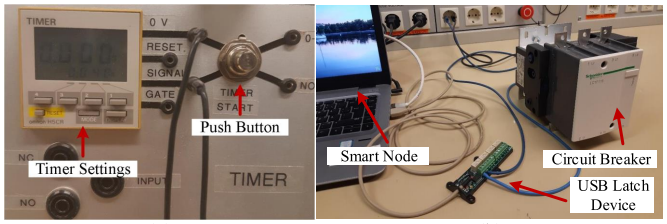

Fig. 18. (a) A picture showing the timer settings, (b) Trip signal setup using the USB latch device and the circuit breaker.

H. Analysis of State Estimation Algorithm

The following aspects related to the SE algorithm are discussed:

- *Robustness*: The WLS SE is robust in its performance and thus it is widely employed. WLS works well with missing measurements similar to other SE techniques assuming that the network observability is maintained. However, bad data detection in WLS SE becomes tedious in the case of multiple bad measurements. In the experimental validation presented in this work, the ratio of a number of measurements (9) to a number of state variables (6) is kept higher i.e., 1.5. The high ratio helps in maintaining the high

redundancy and network observability intact in case of any loss of measurement.

- *Accuracy*: The WLS SE technique has shown good accuracy, as can be seen from Fig. 3 and Fig. 16. During normal operating conditions, the measurements match well with their estimated values and hence could be seen overlapping each other. One of the important factors for SE accuracy is the quality of measurements. In the experimental validation, the measurements are provided with high accuracy from AdvSens due to proper calibration and data conversion strategy. The accuracy of the estimator could be further enhanced with an increased sampling frequency of measurements such as 16 kHz or 32 kHz (currently at 4 kHz).
- *Speed*: A linear version of the WLS SE technique is employed which computes estimates much faster than the non-linear version. In the experimental validation, the average processing time of a sample block has come out to be 12.5 milliseconds. According to current standards related to fault detection and also considering the computational capability of the experimental setup, the estimation speed is in a reasonable range.

I. Comparison between Validation and Simulation Results

The motivation for using the same test case in the simulation and validation studies is to perform a comparison between the two results. Overall, the simulation and validation results have matched very well including the peak values and waveforms during both normal and fault conditions. The following observations could be made using Fig. 3 and Fig. 16:

- *Voltage and Current Waveforms*: The measurements as well as their estimated values from the simulation have matched well with the validation results during the whole simulation time except the post-fault condition. It can be seen from Fig. 19 (for v_a) that the measurements from AdvSens and their estimated values remain in a transient state for the next few cycles after the clearing of the fault unlike the simulation, which could be due to the transient over-voltage in the L-C circuit of the transmission line.
- *Objective Function*: From Fig. 4 and Fig. 17, a higher peak for the objective function can be seen during the fault in the simulation results which is due to a larger mismatch between the measurements and the estimated values of receiving end currents and voltages.

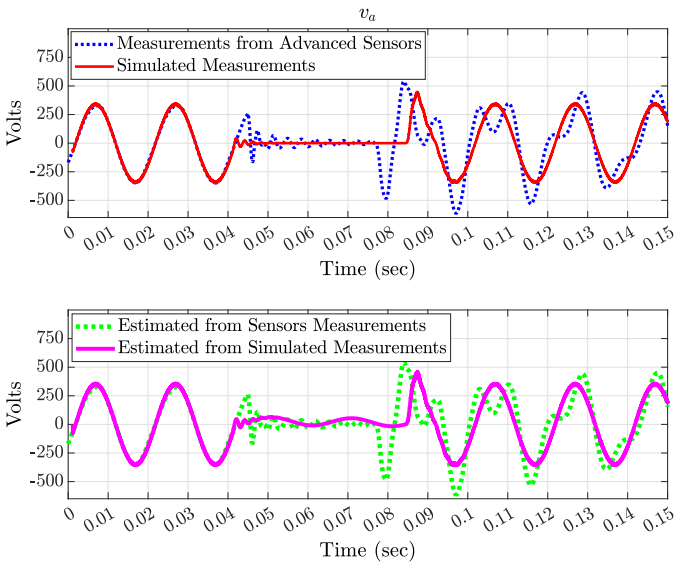

Fig. 19. Comparison plot for measurements and estimated values of receiving end voltage v_a in case of simulation and experimental validation.

It can be inferred from the comparison between the validation and simulation results that the results obtained from the simulation are accurate and closely match the real results obtained from the validation, while the validation results prove that the scheme works as intended in this experimental setup, with the use of AdvSens in case of a particular type of fault. However, more tests would be needed including different types of faults and fault duration.

VII. Fault Detection Time during Experimental Validation

The fault detection time is one of the important features of a protection scheme. The typical fault detection time in the transmission systems with the distance protection is considered to be around 20 to 40 milliseconds in case of 50 Hz system (1 to 2 cycles) depending on the fault location close or further away from the relay. Although in some recent wide-area-based protection approaches, the fault clearing time comes out to be more than 100 milliseconds due to latencies issues [21].

For determining the fault detection time of DSEBPS, the processing time of over 1500 sample blocks is recorded (each sample block contains 40 samples). The processing time of the confidence level is calculated by recording the difference between the time when a sample arrives in the smart node and until the confidence level is produced. The mean and the standard deviation of the processing time of these 1500 sample blocks are calculated using the *normfit* function in MATLAB. The mean value has come out as 12.5 milliseconds. Further, the worst-case and the best case (the maximum and minimum) are recorded as 33.9 milliseconds and 2.89 milliseconds, respectively. The estimated parameters from the *normfit* function are presented in Table III.

TABLE III
Mean and Standard Deviation of Fault Detection Time (in seconds)

Parameter	Value	
Mean	0.0125	
Standard deviation	0.0027	
Lower and upper bounds of the 95% confidence interval for mean	0.0125 (Lower Bound)	0.0125 (Upper Bound)
Lower and upper bounds of the 95% confidence interval for standard deviation	0.0027 (Lower Bound)	0.0028 (Upper Bound)

As mentioned in Section VI-G, the trip signal is generated if the objective function remains above the threshold value for three consecutive samples to have enhanced reliability. With the average processing time of one sample block calculated as 12.5 milliseconds, the maximum average fault detection time will be 25 milliseconds as three samples could be in two different blocks (in the worst case). The fault clearing time composes of fault detection time, communication delay,

and circuit breaker operating time. Since the experimental setup receives the measurements locally, so the communication delays are not considered. The operating time of the circuit breaker is widely considered to be 2 cycles which means 40 milliseconds in a 50 Hz system. With DSEBPS taking 25 milliseconds for fault detection, the fault clearing time comes out approximately to be 65 milliseconds. During validation, each calculation step of the signal value adds a small delay but it is not added separately instead, the complete latency is analyzed by comparing the smart node (laptop) timestamps from the signal arrival until the calculation of the confidence level (which is the last step) is completed. The timestamps of the measurements are re-used for the timestamps of the estimated values, for facilitating the comparison between them for each timestamp. It would be important to highlight here that the computational capabilities of the smart node used in this work could be limited when compared with the industrial-grade smart nodes employed by the power companies.

VIII. Discussion of Protection Performance Under Special Operating Conditions

This section discusses the possible performance of DSEBPS under various special operating conditions. In the future development process, they need to be further examined and tested.

A. CT Saturation Conditions

CT saturation is a common problem in power system protection studies. Many of the newly proposed and as well as existing protection schemes get impacted by this problem. However, there are many practical solutions available for mitigating the CT saturation issue which could also be incorporated in DSEBPS (after detailed investigations) so that it performs as intended even during CT saturation. Some of the solutions could be by employing a higher accuracy class CT [22], reducing CT burden by adding another set of CT cables in parallel, employing percentage differential relay to avoid CT saturation effect, incorporating CT saturation detection algorithms [23], and filtering of decaying DC component and effects of CT saturation using least error squares technique [24]. The recent research works in [25] and [26] employs DSE to detect the CT saturation. Since DSEBPS is also based on DSE, the concept of detecting CT saturation and estimating CT primary current could be easily incorporated in DSEBPS.

B. Evolving Fault

Considering a fault that is initially an external fault and eventually turns into an internal fault [27]. DSEBPS would not detect the external fault even if it is just outside the protection zone as presented in Section V-C. As soon as the fault becomes an internal fault, DSEBPS would detect the fault. In the case when a fault begins as a low-intensity fault (such as high impedance fault) and subsequently develops into a low impedance fault, DSEBPS would detect such fault as it performs well during high impedance fault as presented in Section V-B.

C. Power Swings

Due to power swings, a disturbance in one area could lead to oscillations in generators connected in another area (in the case of an interconnected power system). These oscillations might cause the voltage and currents to start fluctuating. In such conditions, all the measurements including the voltages and currents from local and remote ends of a transmission line would see the same degree of variations. Since the intensity and frequency of power swings are low, the estimated values of the measurements will not have high non-conformity with the measurements like the fault condition. However, during the power swing, the level of conformity will reduce if compared with the normal operating conditions. The non-conformity between the measurements and their estimated values during the power swings could be incorporated using the objective function threshold value and hence the confidence level will remain high and thus DSEBPS will not trigger the tripping.

D. Lightning Surge

Most of the transmission line substations are equipped with a surge arrester (SA) for lightning protection. SAs are installed at the end of the transmission line and between the instrumentation transformers (VTs/CCVTs and CTs) and transmission line [28]. The location of SA ensures that if the lighting occurs at any location of the transmission line then the surge gets arrested by the SA before it can enter VTs/CCVTs and CTs. The modern SA (such as ZnO-arrester) can react very fast, in the order of 10 nanoseconds. If the surge does not enter VTs/CCVTs and CTs, then the corresponding measurements remain unaffected and subsequently, objective function and confidence level also remains unaffected ensuring that DSEBPS works as intended.

E. Switching Phenomenon

Switching phenomenons in power systems could be due to switching on of a transformer leading to inrush current or a large induction motor which could draw heavy currents, etc. Such a phenomenon could lead to the misoperation of protection schemes (e.g., overcurrent, distance relays). Several solutions are proposed in the literature to handle and avoid false tripping, such as the one in [29]. A similar technique could also be tested and applied to DSEBPS. However, such a study is not carried out within the scope of this paper but it is planned to be investigated as part of future studies.

F. Infeed or Outfeed Condition

Infeed or outfeed condition arises due to the line tappings leading to a condition where the distance relay could experience under-reach or over-reach issues and thus negatively impact the tripping decision. In order to investigate this issue, dynamic model of the transmission line was modified to take into account the changes caused due to this condition in the present model. The modifications include new model equations and matrices by incorporating the new branch and currents at the tapped point. Thereafter, a case study was performed with the same test setup but with the incorporation of a tapping point in the middle of the transmission line. This

setup requires more measurements (including phase currents at the tapped point) as compared to the original case study. Due to space limitations, the results from this case study are not included here but the results have proved that DSEBPS works as intended during this condition and the trip signal was successfully generated as the fault was initiated.

G. External Fault with CT Saturation

A few external faults could include e.g., severe CT saturation. The main concern in such a condition is the saturation of only one of the CTs, which could lead to false tripping or sometimes even failure of operation for internal fault under specific conditions [30]. As mentioned previously, DSEBPS is inspired from differential protection which also faces this issue, thus a solution similar to the one proposed in [30] for differential protection could be tested and validated as part of future studies.

IX. Advantages of Open Platform and Real-World Application

A. AdvSens

This subsection discusses the advantages of the open platform from AdvSens perspective. Next to the provided hardware, AdvSens also provides an open platform, which allows third parties to develop their algorithms in common programming languages such as Python and C++. From an innovation perspective, AdvSens and an open platform can be harnessed to produce innovative solutions with a high technology readiness level (TRL).

B. Dynamic State Estimation based Protection Scheme

This subsection discusses the different aspects to be considered for the real-world application of DSEBPS. The implementation of DSEBPS is done using an open platform such as that of AdvSens. The code for DSEBPS is written in an open-source programming language, Python. The Python code of DSEBPS also helps in forming an easy interface to get access to the real-time measurements provided by AdvSens. The following aspects will be important to be considered for real-world application:

- *Communication*: A reliable communication infrastructure is one of the important aspects of DSEBPS implementation. A closed private communication network or wireless communication could be a few of the solutions which could address both communication failures and delay issues. However, the measurement redundancy and pseudo measurements in DSE could also be utilized in some cases of communication failures.
- *Smart Node*: The configuration and location of the smart node are also important aspects for consideration. The smart node should have enough computational power so that the trip signal can be calculated and sent within the standard fault detection time. The location of the smart code could be at one of the substations so that at least one end measurement is locally received.
- *CTs and VTs/CCVTs Calibration*: For the application of AdvSens in high voltage transmission lines, metering transformers (such as CTs and VTs/CCVTs) are needed to be installed for conversion of the high voltages and currents to the measurement level [31]. A secondary stage calibration procedure could also be used for correcting the phase and voltage displacement of the signals provided that the calibration parameters are known within AdvSens.
- *Primary or Backup Protection Scheme*: DSEBPS could first be used as a backup protection scheme and after satisfactory implementation and validation spanning over a few years, it could be employed as a primary protection scheme.

X. Conclusion

The paper concludes that the application of DSE-based protection on a transmission line works satisfactorily in both simulation and experimental validation setup. It further suggests that the scheme performed adequately both in terms of selectivity and time. The experimental setup does not generate a trip signal during the normal operating conditions (avoids unwanted tripping) , while the trip signal is successfully generated during the fault condition. The application of AdvSens has also been validated which worked as the key component in the scheme providing an opportunity to be rolled out as a commercial product. The DSE and AdvSens integration in the open platform works well and could contribute to more development in the future. The key takeaways from the paper are the absence of complex relay settings and lack of coordination in DSEBPS which could lead to a substantial reduction in misoperations due to incorrect relay settings (which is one of the major causes of misoperations). The work conducted in this paper has led to the identification of several new areas for development and validation within DSEBPS. The future work could involve evaluating the performance of AdvSens (such as accuracy, latency, etc.) when they are connected with protection class instrumentation transformer in a real high voltage transmission line, carrying out validation for more case studies to evaluate performance under different fault types. Further, the more in-depth investigations on the performance of DSEBPS with CT saturation, power swings, lightning surge, switching phenomenons in power systems, and, external fault with CT saturation.

Acknowledgement

The authors would like to thank the anonymous reviewers for their valuable comments and suggestions which helped improve the clarity and quality of the paper.

References

[1] NERC, "Analysis of system protection misoperations," Dec. 2015.
[2] A. P. S. Meliopoulos *et al.*, "Dynamic state estimation-based protection: Status and promise," *IEEE Transactions on Power Delivery*, vol. 32, no. 1, pp. 320–330, 2016.
[3] Z. Y. Xu, Z. Q. Du, L. Ran, Y. K. Wu, Q. X. Yang, and J. L. He, "A current differential relay for a 1000-kV UHV transmission line," *IEEE Transactions on Power Delivery*, vol. 22, no. 3, pp. 1392–1399, 2007.
[4] J. Zhao *et al.*, "Power system dynamic state estimation: Motivations, definitions, methodologies, and future work," *IEEE Transactions on Power Systems*, vol. 34, no. 4, pp. 3188–3198, 2019.
[5] A. P. S. Meliopoulos *et al.*, "Setting-less protection: Feasibility study," in *Proc. 46th IEEE Hawaii Intl. Conf. on Sys. Sci.*, 2013, pp. 2345–2353.
[6] Y. Liu, A. P. S. Meliopoulos, R. Fan, L. Sun, and Z. Tan, "Dynamic state estimation based protection on series compensated transmission lines," *IEEE Trans. on Power Delivery*, vol. 32, no. 5, pp. 2199–2209, 2016.

[7] J. Xie, A. P. S. Meliopoulos, and B. Xie, "Transmission line fault classification based on dynamic state estimation and support vector machine," in *Proc. IEEE North American Power Symposium (NAPS)*, 2018, pp. 1–5.

[8] H. F. Albinali and A. P. S. Meliopoulos, "Resilient protection system through centralized substation protection," *IEEE Transactions on Power Delivery*, vol. 33, no. 3, pp. 1418–1427, 2018.

[9] D. Rimorov, Y. Brissette, I. Kamwa, and G. Joós, "Synchrophasor-based state estimation for microgrid protection," in *Proc. IEEE Power & Energy Society General Meeting*, 2018, pp. 1–5.

[10] Y. Cui, R. Kavasseri, and S. Brahma, "Dynamic state estimation assisted posturing for generator out-of-step protection," in *Proc. IEEE Power and Energy Society General Meeting*, 2016, pp. 1–5.

[11] B. Wang, Y. Liu, D. Lu, K. Yue, and R. Fan, "Transmission line fault location in MMC-HVDC grids based on dynamic state estimation and gradient descent," *IEEE Transactions on Power Delivery*, vol. 36, no. 3, pp. 1714–1725, 2020.

[12] Shalini *et al.*, "Enhancing performance of wide-area back-up protection scheme using PMU assisted dynamic state estimator," *IEEE Trans. on Smart Grid*, vol. 10, no. 5, pp. 5066–5074, 2018.

[13] Y. Liu *et al.*, "Dynamic state estimation for power system control and protection," *IEEE Transactions on Power Systems*, vol. 36, no. 6, pp. 5909–5921, 2021.

[14] UNITED-GRID, [Online] Available: https://united-grid.eu/.

[15] Y. H. Lee, "A comprehensive protection scheme for distribution systems," Ph.D. dissertation, Georgia Institute of Technology, 2014.

[16] A. P. Meliopoulos, G. J. Cokkinides, and G. K. Stefopoulos, "Quadratic integration method," in *Proc. Citeseer International Power System Transients Conference (IPST)*, 2005, pp. 19–23.

[17] A. Srivastava, "Towards intelligent distribution systems: Solutions for congestion forecast and dynamic state estimation based protection," Licentiate Thesis, Chalmers University of Technology, 2021.

[18] Smart State Technology, The Netherlands, [Online] Available: https://www.smartstatetechnology.nl/.

[19] D. Ritzmann, P. S. Wright *et al.*, "A method for accurate transmission line impedance parameter estimation," *IEEE Transactions on Instrumentation and Measurement*, vol. 65, no. 10, pp. 2204–2213, 2016.

[20] R. Mohanty and A. K. Pradhan, "Protection of smart DC microgrid with ring configuration using parameter estimation approach," *IEEE Transactions on Smart Grid*, vol. 9, no. 6, pp. 6328–6337, 2017.

[21] J. G. Rao and A. K. Pradhan, "Supervising distance relay during power swing using synchrophasor measurements," *IET Generation, Transmission & Distribution*, vol. 11, no. 17, pp. 4136–4145, 2017.

[22] A. Hargrave, M. J. Thompson, and B. Heilman, "Beyond the knee point: A practical guide to CT saturation," in *Proc. IEEE 71st Annual Conference for Protective Relay Engineers (CPRE)*, 2018, pp. 1–23.

[23] Y.-C. Kang, S.-H. Ok, and S.-H. Kang, "A CT saturation detection algorithm," *IEEE Transactions on Power Delivery*, vol. 19, no. 1, pp. 78–85, 2004.

[24] A. Hooshyar and M. Sanaye-Pasand, "Accurate measurement of fault currents contaminated with decaying DC offset and CT saturation," *IEEE Transactions on Power Delivery*, vol. 27, no. 2, pp. 773–783, 2012.

[25] P. E. Obikwelu and A. P. S. Meliopoulos, "VT instrumentation channel error correction using dynamic state estimation," in *Proc. IEEE 52nd North American Power Symposium (NAPS)*, 2021, pp. 1–6.

[26] P. E. E. Obikwelu and A. P. S. Meliopoulos, "CT saturation error correction within merging units using dynamic state estimation," in *Proc. IEEE 3rd International Conference on Renewable Energy and Power Engineering (REPE)*, 2020, pp. 45–50.

[27] F. A. M. Vásquez and K. M. Silva, "Instantaneous-power-based busbar numerical differential protection," *IEEE Transactions on Power Delivery*, vol. 34, no. 2, pp. 616–626, 2019.

[28] S. A. Hosseini, M. Mirzaie, and T. Barforoshi, "Impact of surge arrester number and placement on reliability and lightning overvoltage level in high voltage substations," *International Journal of Electrical Power & Energy Systems*, vol. 65, pp. 146–158, 2015.

[29] B. Kasztenny, "Impact of transformer inrush currents on sensitive protection functions," in *Proc. IEEE Transmission and Distribution Conference and Exhibition*, 2006, pp. 820–823.

[30] S. AsghariGovar and H. Seyedi, "Adaptive CWT-based transmission line differential protection scheme considering cross-country faults and CT saturation," *IET Generation, Transmission & Distribution*, vol. 10, no. 9, pp. 2035–2041, 2016.

[31] H. E. V. Brom *et al.*, "Voltage dependence of the reference system in medium-and high-voltage current transformer calibrations," *IEEE Trans. on Instrumentation and Measurement*, vol. 70, pp. 1–8, 2021.

Ankur Srivastava (Student Member, IEEE) received the M.Tech degree in 2015 from the National Institute of Technology Warangal, Telangana, India, in Electrical Engineering. He worked as a Graduate Engineer in SMS India Private Limited, India from 2011 to 2012 and as a Research Associate in the Department of Electrical Engineering, Indian Institute of Technology, Kanpur, India from 2016 to 2017.

Currently, he is working towards his Ph.D. degree in the Division of Electric Power Engineering, Department of Electrical Engineering, Chalmers University of Technology, Gothenburg, Sweden since 2017. His research interests include power system state estimation, power system protection, and renewables integration in distribution systems.

Le Anh Tuan (Member, IEEE) received the B.Sc. degree in power systems from the Hanoi University of Technology, Vietnam, in 1995, the M.Sc. degree in energy economics from the Asian Institute of Technology, Bangkok, Thailand, in 1997, and the Ph.D. degree in power systems from the Chalmers University of Technology, Gothenburg, Sweden, in 2004, where he is currently an Associate Professor with the Division of Electric Power Engineering, Department of Electrical Engineering. His current research interests include, modelling, optimization, control and protection of integrated energy systems, and active distribution networks with high level of renewables and energy storage, wide-area monitoring and control of large power transmission systems, machine learning applications to power systems, modelling and design of energy and ancillary service markets.

David Steen received the M.Sc. and Ph.D. degrees in electrical engineering from the Chalmers University of Technology, Gothenburg, Sweden, in 2008 and 2014, respectively, where he is currently a Researcher with the Department of Electrical Engineering. His research interests include modelling and control of integrated energy systems and distributed energy resources such as solar PV, wind power, electric vehicles, and energy storage.

Ola Carlson was born in Onsala, Sweden, in 1955. He received the M.Sc. and Ph.D. degrees in electrical engineering from the Chalmers University of Technology, Gothenburg, Sweden, in 1980 and 1988, respectively, where he is currently a Professor with the Department of Electrical Engineering. His major interests are electrical systems for renewable power production and hybrid electric vehicles.

Omar Mansour is co-owner and co-founder of Smart State Technology BV, The Netherlands. He is a researcher and R&D Manager with 20 years of experience in the field of hardware and system development. He has been involved in the development of various centralized substation automation systems for secondary substations and various smartgrid industrial research projects with partners such as Alliander (NL), 3M (DE), Smarter Grid Solutions (UK), Fortum and Protrol (SE).

Dennis Bijwaard is a co-owner and co-founder of Smart State Technology BV, The Netherlands. He managed and participated in R&D projects on wired/wireless electrical, environmental and motion sensing solutions (Locamation, Ambient Systems, Inertia Technology, Fusion Electronics, Alcatel-Lucent). Dennis holds a PhD from the University of Twente on "Real-time Mobile Sharing of Multimedia and Context".